Journal of Alloys and Compounds 509 (2011) 6987–6993

Contents lists available at ScienceDirect

Journal of Alloys and Compounds

journal homepage: www.elsevier.com/locate/jallcom

Infrared spectroscopic properties of Tm^{3+}, Ho^{3+}:$NaY(WO_4)_2$ single crystals

Chengli Sun[a,b], Fugui Yang[a,b], Ting Cao[a,b], Zhenyu You[a], Yan Wang[a], Jianfu Li[a], Zhaojie Zhu[a], Chaoyang Tu[a,*]

[a] Key Laboratory of Optoelectronic Materials Chemistry and Physics of CAS, Fujian Institute of Research on the Structure of Matter, Chinese Academy of Sciences, Fuzhou City, Fujian Province 350002, People's Republic of China
[b] Graduate School of Chinese Academy of Sciences, Beijing 100039, People's Republic of China

ARTICLE INFO

Article history:
Received 11 August 2010
Received in revised form 19 March 2011
Accepted 25 March 2011
Available online 1 April 2011

Keywords:
Tm^{3+}
Ho^{3+}:$NaY(WO_4)_2$ crystals
Optical spectroscopies

ABSTRACT

Singly doped and Tm^{3+}/Ho^{3+} co-doped $NaY(WO_4)_2$ single crystals were grown successfully by Czochralski method. The room temperature polarized absorption and fluorescence spectra as well as the decay curves were measured. Spectroscopic parameters related to the laser operation around 2.0 μm via the $^3F_4 \rightarrow {}^3H_6$ (Tm^{3+}) and $^5I_7 \rightarrow {}^5I_8$ (Ho^{3+}) transitions have been evaluated. The energy level scheme and energy transfer processes of Tm^{3+} and Ho^{3+} were analyzed.

1. Introduction

Laser emissions of around 2.0 μm in the eye-safe spectral region possesses many features, which makes it attractive for lidar, remote sensing, medicine and environmental gas detection research since the 1970s [1–6]. Singly doped thulium (Tm) and holmium (Ho), as well as co-doped Tm:Ho systems have been investigated for this purpose. Tm^{3+} can be pumped directly with 800 nm AlGaAs diode lasers through the $^3H_6 \rightarrow {}^3H_4$ transition and a cross-relaxation mechanism populates the $^3F_4$ multiplet. Laser emission of Tm^{3+} occurs near 2.0 μm due to the $^3F_4 \rightarrow {}^3H_6$ de-excitation. Moreover, Tm^{3+} is also a sensitizer of Ho^{3+} leading to an enhancement of the spectral range of laser emission [7]. It transfers its excitation to Ho^{3+}.$^5I_7$ multiplet from which the 2.06 μm laser originates. High-gain cross section and the long lifetime of the $^5I_7$ upper laser level is a significant advantage of Ho^{3+} for laser operation at 2 μm [8].

The first demonstration of laser emission performed at Bell Laboratories in 1962 was that Johnson et al. produced stimulated emission at 1.91 μm of Tm^{3+} and Ho^{3+} at 2.06 μm in $CaWO_4$ crystals at 77K [9]. The first report of room-temperature Tm^{3+} laser operation around 2 μm was Cr^{3+}/Tm^{3+}:YAG and Cr^{3+}/Tm^{3}:$YAlO_3$ in 1975 [10]. Due to the lack of an appropriate pump source in the following period, Tm^{3+} ions were generally sensitized by Cr^{3+} or Er^{3+}, which can efficiently be pumped by flash-lamps or Ar gas lasers. A real breakthrough arrived with the development of AlGaAs laser diodes emitting in the 800 nm region. Room-temperature laser operation at 2 μm has been achieved in numerous Tm^{3+}-doped and Ho^{3+}-doped crystals, such as aluminates (Tm^{3+}:YAG) [11], double tungstates (Tm^{3+}:NLuW) [12], vanadates (Tm^{3+}:YVO_4) [13], and fluorides (Tm^{3+}:BaY_2F_8) [14].

The lattice parameters of $NaY(WO_4)_2$ crystal are $a = b = 5.205$ Å and $c = 11.251$ Å, respectively with the space group of $I4_1/a$ [15]. This crystal is a typical tetragonal scheelite-type crystal with a formula $MT(WO_4)_2$, where M is a monovalent alkali cation and T a trivalent cation. In these materials the M and T cations are randomly distributed in the 2b and 2d sites [16]. As a consequence, the optical absorption and emission lines become broadened, which allow some laser tunability as well as a better match with the available diode laser emissions used for pumping. As it melts congruently, large size single crystal can be easily obtained by the Czochralski (CZ) method.

We have demonstrated an infrared laser output at 2.07 μm with Tm, Ho co-doped $NaY(WO_4)_2$ crystal with an end-pumped configuration using a 795 nm laser diode at 283 K [17]. In this paper, we present room temperature absorption spectra, fluorescence spectra and luminescence decay curves of Tm^{3+}, Ho^{3+} singly doped and Tm^{3+}/Ho^{3+} co-doped $NaY(WO_4)_2$ crystals. Room temperature absorption spectrum were applied to Judd–Ofelt (J–O) analysis [18,19] to calculate spectral parameters. Spectroscopic parameters related to the laser operation around 2.0 μm have been evaluated.

2. Experimental

2.1. Crystal growth

$NaY(WO_4)_2$ single crystals were grown using the Czochralski technique in air. The polycrystalline materials used for single crystals growth were obtained by clas-

* Corresponding author. Tel.: +86 591 83711368; fax: +86 591 8371 4946.
E-mail address: tcy@fjirsm.ac.cn (C. Tu).

0925-8388/$ – see front matter © 2011 Elsevier B.V. All rights reserved.
doi:10.1016/j.jallcom.2011.03.143

sical solid-state reaction. The initial chemicals of Na_2CO_3 (99.99%), Y_2O_3 (99.99%), WO_3 (99.99), Tm_2O_3 (99.99%) and Ho_2O_3 (99.99%) powders were mixed in an agate mortar in stoichiometric amounts, all the reagents were purchased from Sinopharm Chemical Reagent Co. Ltd. These materials were pressed into tablets and sintered to obtain single phase powder. In the DJL-400 furnace they were heated 50 °C higher than the melting temperature of 1210 °C for about 1 h so as to melt completely and homogeneously. During crystal growth, the Pt rod was rotated at a rate of 12.0–20.0 rpm and the pulling rate was 0.8–1.2 mm/h. When the growth process was over, the crystals were drawn out of the melt and cooled down to room temperature at a rate of 12.0–30.0 °C/h.

The concentration of doping ions in the crystals was measured by the inductively coupled plasma-atomic emission spectrometry (ICP-AES) method. The doping ions concentration in the melt, N_0, the average doping ions concentration in the crystal, N_c, and the segregation coefficient of the doping ions in crystals, K, are given in Table 1.

2.2. Spectroscopic measurements

Room temperature polarized absorption spectra were measured in the range from 300 to 2200 nm by using a Perkin-Elmer UV-VIS-NIR Spectrometer (Lambda-900). The room temperature fluorescence spectra ranging from 1600 to 2300 nm and the luminescent decay curves were recorded with an Edinburgh Instruments FSP920 spectrophotometer. The samples used for spectroscopic measurements were optically polished to flat and parallel faces. In order to reduce the reabsorption on the fluorescence, the lifetime measurements were carried out with fine powdered Tm^{3+}, Ho^{3+} doped $NaY(WO_4)_2$ crystals immersed in monochlorobenzene.

3. Results and discussions

3.1. Absorption spectra

Fig. 1 shows the polarized absorption spectra measured at room temperature for the Tm^{3+}, Ho^{3+} singly doped and Tm^{3+}/Ho^{3+} co-doped $NaY(WO_4)_2$ crystals. The spectrum of Tm^{3+}:$NaY(WO_4)_2$ crystal consists of six resolved bands associated with the transitions from the $^3H_6$ ground state to the $^3F_4$, $^3H_5$, $^3H_4$, $^3F_{2,3}$, $^1G_4$ and $^1D_2$ excited states. It can be seen that the absorption band of the σ polarization is narrower and has a larger peak cross section than the π absorption band. The spectrum of Ho^{3+}:$NaY(WO_4)_2$ crystal consists of ten resolved bands associated with the transitions from the $^5I_8$ ground state to the $^5I_7$, $^5I_6$, $^5F_5$, $^5F_4+{}^5S_2$, $^5F_3$, $^3K_8+{}^5F_2$, $^5F_1+{}^5G_6$, $^5G_5(^3G_5)$, $^3H_6+{}^5F_2+{}^3H_5$ and $^3K_6+{}^3F_4+{}^3H_4+{}^3G_4$ excited states [20]. Some absorption bands of Tm^{3+} and Ho^{3+} ions overlap in the Tm^{3+}/Ho^{3+}:$NaY(WO_4)_2$ crystal. Compared to Ho^{3+} ions concentration in Ho^{3+}:$NaY(WO_4)_2$ and Tm^{3+} ions concentration in Tm^{3+}/Ho^{3+}:$NaY(WO_4)_2$ crystal, the concentration of Ho^{3+} ions in Tm^{3+}/Ho^{3+}:$NaY(WO_4)_2$ crystal is very low; the $^5I_8 \rightarrow {}^5I_7$ (Ho^{3+}) transition of Tm^{3+}/Ho^{3+}:$NaY(WO_4)_2$ crystal is extremely weak. The absorption cross sections σ_a can be determined by the following equation:

$$\sigma_a = \frac{\alpha}{N_c} \tag{1}$$

Here α is the absorption coefficient, $\alpha = A/(L \times \log_{10} e)$, A is the absorbance, L is the thickness of the polished crystal, and N_c is the doping ions concentration in $NaY(WO_4)_2$ crystal. The absorption cross sections and the full width at half maximum (FWHM) for some absorption bands of these crystals are shown in Table 2. There is a relative broad and strong absorption band at about 795 nm of the $^3H_6 \rightarrow {}^3H_4$ (Tm^{3+}) transition, which is suitable for the AlGaAs diode pumping. This absorption cross section values are similar to those for Tm:KGdW [21]. For Ho^{3+}, the absorption peak at 452 nm is far stronger than the others. As a consequence, Ho^{3+}:$NaY(WO_4)_2$ crystal is prone to be pumped by visible light, such as Ar gas laser.

From the absorption, we can use the reciprocity method to calculate the theoretical emission cross-sections of the Tm^{3+} ion $^3F_4 \rightarrow {}^3H_6$ transition [22]:

$$\sigma_{em}(\lambda) = \sigma_a(\lambda)\frac{Z_l}{Z_u}\exp\left[\frac{E_{ZL} - hc/\lambda}{k_B T}\right] \tag{2}$$

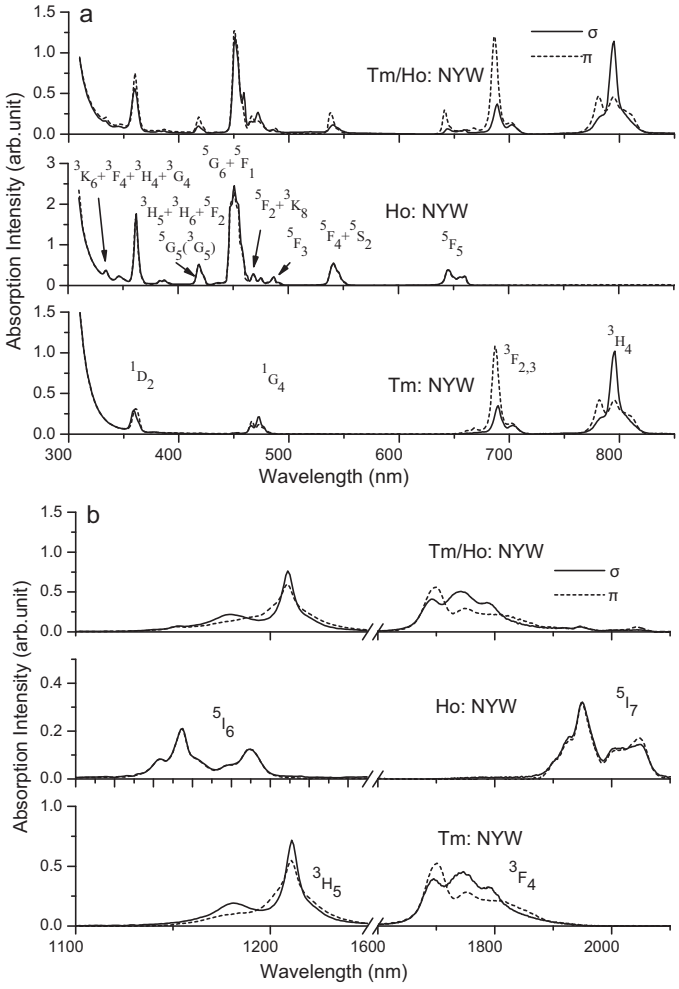

Fig. 1. (a) Room temperature absorption spectra of Tm^{3+}-, Ho^{3+}-doped and Tm^{3+}/Ho^{3+} co-doped $NaY(WO_4)_2$ crystals in the range 300–850 nm and (b) in the range 1100–2100 nm.

where $\sigma_a = \alpha/N_c$ is the absorption cross-section, and $Z_{l,u} = \sum kg_k \exp(-E_k/k_B T)$ are the partition functions of the $^3H_6$ and $^3F_4$ multiplet, where g_k is the level degeneracy, E_k is the energy difference with respect to the lowest Stark level, k_B is the Boltzmann constant, T is the temperature, and E_{ZL} is the zero line, which is the energy separation between the lowest crystal-field components of the lower and upper manifolds. However, due to the lack of low temperature equipment, the precise energy scheme of Tm^{3+}:$NaY(WO_4)_2$ cannot be obtained at present. The values of Z_l/Zu and E_{ZL} were estimated to be 1.35 and 5591 cm^{-1}, respectively, which is of the order of those of Tm^{3+}:NGW [23], Tm^{3+}:NLuW [12], Tm^{3+}:$KLa(WO_4)_2$ [24], Tm^{3+}:$KGd(WO_4)_2$ [25] and Tm^{3+}:$KY(WO_4)_2$ [26] crystals. Fig. 2 shows the σ_{abs} and σ_{em}. The maximum values of σ_{em} are 1.399×10^{-20} cm^2 for σ polarization at 2044 nm and 1.426×10^{-20} cm^2 for π polarization at 2047 nm. For comparison, the σ_{em} obtained for Tm^{3+} in NLuW are $2.0(\pm 0.1) \times 10^{-20}$ cm^2 at 1798 nm and $1.9(\pm 0.1) \times 10^{-20}$ cm^2 at 1830 nm, respectively [12]. The FWHMs of the emission bands for σ and π polarizations are 161 and 130 nm, respectively.

The tunable range of the $^3F_4 \rightarrow {}^3H_6$ laser operation could be evaluated from the gain cross section σ_{gain} which is defined as

$$\sigma_{gain} = P\sigma_{em}(\lambda) - (1-P)\sigma_a(\lambda) \tag{3}$$

where P is the population inversion parameter, defined as the density of excited Tm^{3+} ions divided by the doping concentration N_0.

Table 1
The ions concentrations and segregation coefficient of the doping in crystals. N_0: concentration of the doping ions in the melt; N_c: average concentration of the doping ions in the crystal.

Crystal	N_0 (at.%)	N_c ($\times 10^{20}$ ions cm^{-3})	K
Tm^{3+}:$NaY(WO_4)_2$	5	2.596	0.22
Ho^{3+}:$NaY(WO_4)_2$	5	2.466	0.204
Tm^{3+}/Ho^{3+}:$NaY(WO_4)_2$	5 (Tm)	2.69 (Tm)	0.23 (Tm)
	1 (Ho)	0.58 (Ho)	0.24 (Ho)

Table 2
The absorption cross sections and the full width at half maximum (FWHM) for some absorption bands.

Crystal	λ (nm)		FWHM (nm)		σ_a ($\times 10^{-20}$ cm^2)	
	σ	π	σ	π	σ	π
Tm^{3+}:$NaY(WO_4)_2$	795	794	8	35	3.818	1.685
Ho^{3+}:$NaY(WO_4)_2$	451	452	8	7	18.497	17.972
Tm^{3+}/Ho^{3+}:$NaY(WO_4)_2$	795	795	9	35	4.101	1.695

Gain cross-section σ_{gain} calculated for several reasonable values of P (P = 0.1, 0.2, 0.3, 0.4, 0.5) in the 1700–2000 nm region are shown in Fig. 3. The gain curves at a wavelength longer than 1900 nm are obscure due to the low signal-to-noise ratio of the absorption spectrum. The positive gain cross-section can be obtained at about 2.0 μm when P exceeds 0.2. The positive gains for P = 0.5 are in a range from 1758 to about 1954 nm for σ polarization and from 1758 to about 1977 nm for π polarization, respectively.

We also calculated the theoretical emission cross-sections together with the gain cross section of the emitting Ho^{3+} transition $^5I_7 \rightarrow {}^5I_8$ [shown in Figs. 2(b) and 3(b)]. The maximum values of σ_{em} is 2.162×10^{-20} cm^2 for σ polarization at 1795 nm and 2.031×10^{-20} cm^2 for π polarization at 1841 nm. Table 3 shows the results and comparisons with other hosts. The FWHMs of the emission bands for σ and π polarizations are nearly 251 nm. The positive gain cross-section can be obtained at about 2.0 μm when the P exceeds 0.3, then laser operation should be achievable in the 1960–2112 nm range.

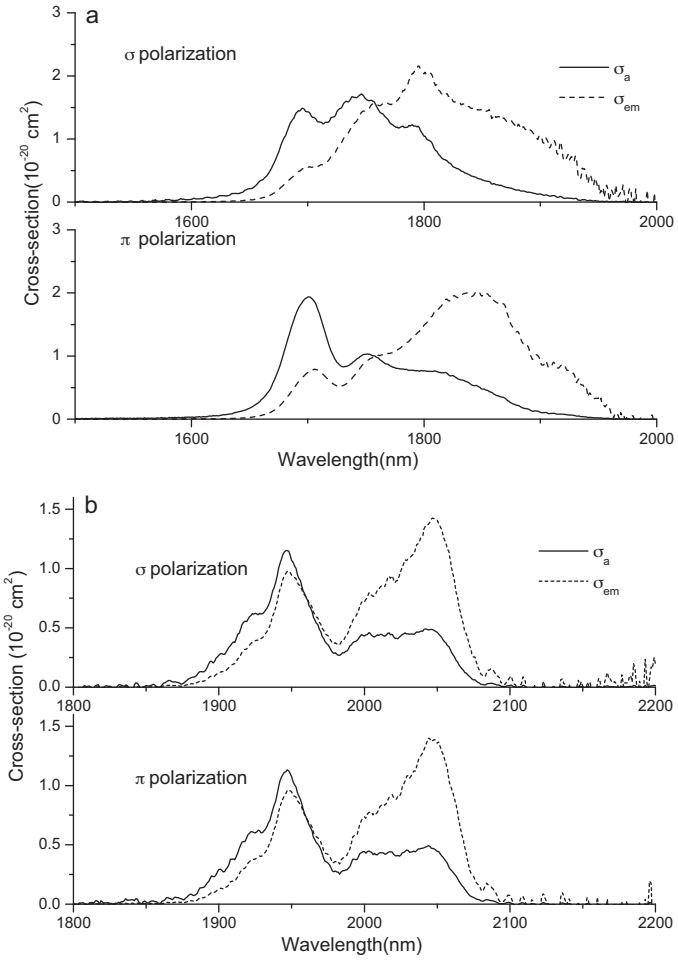

Fig. 2. Absorption cross sections and polarized stimulated emission cross sections associated with the (a) $^3F_4 \rightarrow {}^3H_6$ transition for the Tm^{3+}:$NaY(WO_4)_2$ and (b) $^5I_7 \rightarrow {}^5I_8$ for Ho^{3+}:$NaY(WO_4)_2$ crystal derived by the reciprocity method.

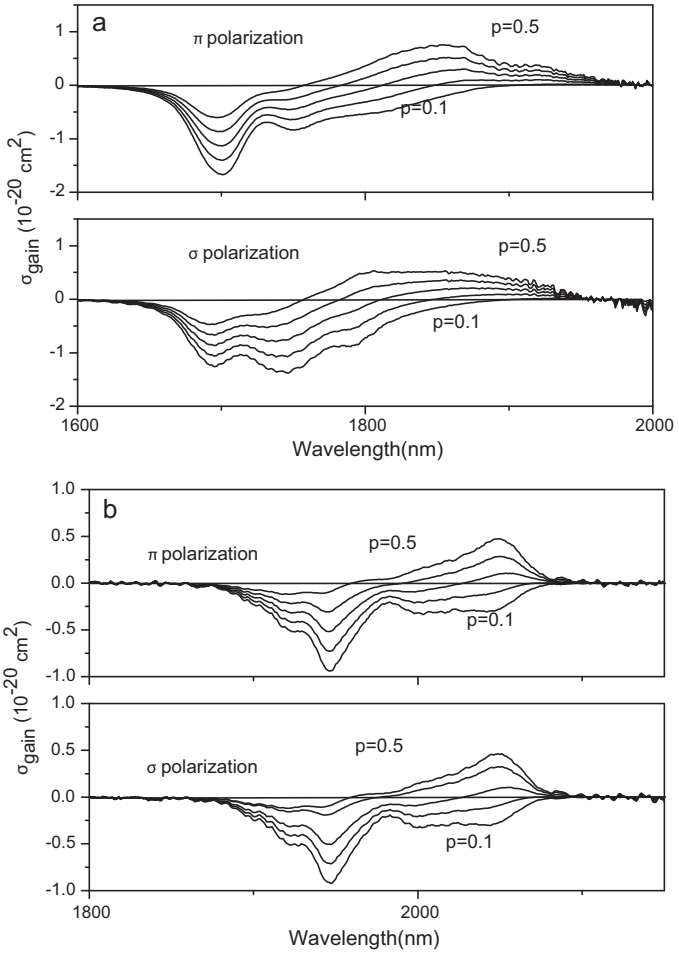

Fig. 3. Gain cross-section calculated for different values of P (P = 0.1–0.5) for (a) the $^3F_4 \rightarrow {}^3H_6$ transition of Tm^{3+} in $NaY(WO_4)_2$ crystal and (b) the $^5I_7 \rightarrow {}^5I_8$ transition of Ho^{3+} in $NaY(WO_4)_2$ crystal.

Table 3
The emission cross sections in several solid-state materials.

(Tm, Ho):host	σ_e ($\times10^{-20}$ cm^2) $^3F_4 \rightarrow {}^3H_6$ (λ_e, nm)	σ_e ($\times10^{-20}$ cm^2) $^5I_7 \rightarrow {}^5I_8$ (λ_e, nm)	[Ref]
Tm:NYW	2.16 (σ, 1795) 2.03 (π, 1845)	/	This work
Ho:NYW	/	1.43 (σ, 2047) 1.40 (π, 2044)	This work
Tm, Ho:NYW	/	1.43 (σ, 2042) 0.54 (π, 2044)	This work
YAG	0.22[a] (2011)	0.98[a] (2100) 0.9 (2091)	[24]
BaYF	0.25[a] (1919)	1.01[a] (2057)	[24]
Tm:NLaM	1.91 (σ, 1789) 1.96 (π, 1837)	/	[18]
Tm, Ho:KGdW	/	2.94 (E//Nm, 2019) 1.33 (E//Np, 2054)	[24]
YVO4	2.60[a] (E//c, 1805) 1.73[a] (E⊥c, 1804)	2.6[a] (E//π, 2038) 1.8[a] (E//σ, 2010)	[24]

[a] Singly-doped values.

3.2. The Judd–Ofelt analysis

The Judd–Ofelt (J–O) theory was applied to calculate the spectral parameters, including the line strength S, the radiative rate A, the branching ratio β and the radiative lifetime τ_r of some typical transitions levels. Lots of literature have described the calculation process of the J–O theory details [28–31]. The Judd–Ofelt (J–O) theory analysis of the Tm^{3+}:$NaY(WO_4)_2$, Ho^{3+}:$NaY(WO_4)_2$ crystal are shown in Tables 3–6. The effective J–O intensity parameters were calculated following $\Omega_{eff} = (2\Omega_\sigma + \Omega_\pi)/3$. It was reported that Ω_2 is structure sensitive and associated with the asymmetry and covalence of the lanthanide sites [32]. The small value of Ω_2 indicates that there is a high asymmetry and a weak covalent bond character for the doping ions in this crystal. Two other parameters are also useful in calculating the spectroscopic quality factor $X = \Omega_4/\Omega_6$, which plays an important role in predicting the stimulated emission for the laser active media [32]. Generally, the preferred laser materials should be those possessing large X values.

3.3. Fluorescence spectra

Since the lack of polarizer, we just recorded the room temperature unpolarized fluorescence spectra ranging from 1600 nm to 2300 nm under the 794 nm pumping shown in Fig. 4. These crystals are promising for tunable emission due to their large emission bandwidth. In Tm^{3+} doped crystals the emission band ranges from 1650 to 2138 nm, which is almost 488 nm of possible tunability. For Ho^{3+}:$NaY(WO_4)_2$, that is in the 1834–2200 nm region.

Owing to the radiative-trapping, the lifetime measurements were carried out with fine powdered Tm, Ho doped $NaY(WO_4)_2$ crystals immersed in monochlorobenzene, which was used as the refractive index matching fluid to minimize the reabsorption in the particles and contained in a glass cuvette [33]. For comparison, we also tested the bulk samples of Tm^{3+}:$NaY(WO_4)_2$ crystal. The room temperature fluorescence decay of the $^3F_4$ (Tm^{3+}) was measured at 1860 nm under excitation at 794 nm. The fluorescence lifetime could be estimated by

$$\tau_f = \frac{\int_0^\infty tI(t)\mathrm{d}t}{\int_0^\infty I(t)\mathrm{d}t} \quad (4)$$

where $I(t)$ is the fluorescence intensity at time t. The room temperature fluorescence decay of the $^3F_4$ (Tm^{3+}) was measured at 1860 nm under excitation at 794 nm. Shown in Fig. 5, the calculated fluorescence lifetime of $^3F_4$ (Tm^{3+}) manifold in bulk sample (2.441 ms) is much longer than in powder (1.267 ms). Compared to the radiative lifetime calculated based on the Judd–Ofelt (J–O) theory, 1.308 ms, the powder sample's lifetime is reasonable. The fine powder efficiently eliminated the influence of luminescence re-absorption.

We measured the decay of the $^5I_7$ level of Ho^{3+} with Ho^{3+}:$NaY(WO_4)_2$ and Tm^{3+}, Ho^{3+}:$NaY(WO_4)_2$ at 2045 nm under 452 nm excitation and Tm^{3+}, Ho^{3+} co-doped $NaY(WO_4)_2$ crystal powder at 2045 nm under 794 nm excitation. The decay curves are shown in Fig. 6. The fluorescence lifetimes τ_f are3.44 ms and 3.122 ms, respectively, which are close to that in the Ho, Tm:KGdW (3.15–5.17 ms) and Ho:YVO_4 (3.8 ms) crystals [27].

Table 4
The Judd–Ofelt intensity parameters of Tm^{3+} and Ho^{3+} doped $NaY(WO_4)_2$ crystal.

	Intensity		
	σ polarized	π polarized	Effective
Parameter (Tm^{3+})			
Ω_2	13.845	9.465	12.385
Ω_4	2.463	3.545	2.824
Ω_6	1.286	3.058	1.877
X	/	/	1.505
Parameter (Ho^{3+})			
Ω_2	19.795	18.316	19.302
Ω_4	3.967	5.766	4.567
Ω_6	2.093	1.986	2.057
X	/	/	2.22

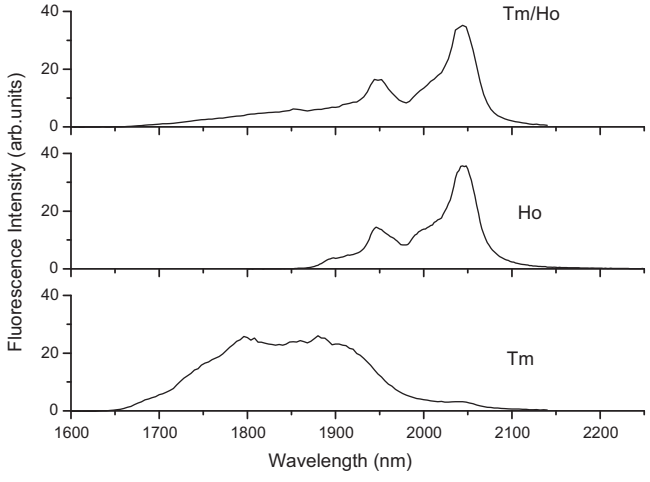

Fig. 4. Room temperature fluorescence spectra of Tm^{3+}-, Ho^{3+}-doped and Tm^{3+}/Ho^{3+} co-doped $NaY(WO_4)_2$ crystals.

Table 5
The experimental and calculated absorption line and oscillator strengths of the Tm^{3+}:$NaY(WO_4)_2$ crystal and Ho^{3+}:$NaY(WO_4)_2$ at room temperature.

Tm^{3+}	λ	σ polarized				λ	π polarized			
$^3H_6\rightarrow$	(nm)	S_{exp} (10^{-20} cm^2)	S_{calc}	f_{exp} (10^{-6})	f_{calc}	(nm)	S_{exp} (10^{-20} cm^2)	S_{calc}	f_{exp} (10^{-6})	f_{calc}
$^1D_2$	366	1.19	0.89	5	3.76	362	1.41	1.40	5.98	5.95
$^1G_4$	478	0.95	0.87	3.07	2.79	474	0.96	0.76	3.12	2.46
$^3F_{3,2}$	685	2.00	2.19	4.49	4.92	685	4.65	4.48	10.42	10.05
$^3H_4$	796	4.53	4.32	8.74	8.33	794	4.56	4.45	8.81	8.61
$^3H_5$	1204	3.01	2.88	3.84	3.67	1202	3.40	3.79	4.35	4.84
$^3F_4$	1748	9.41	9.54	8.27	8.38	1752	8.40	8.39	7.37	7.36
		rmsΔS = 0.265		rmsΔf = 0.818			rmsΔS = 0.276		rmsΔf = 0.534	

Ho^{3+}	λ	σ polarized				π polarized			
$^5I_8\rightarrow$	(nm)	S_{exp} (10^{-20} cm^2)	S_{calc}	f_{exp} (10^{-6})	f_{calc}	S_{exp} (10^{-20} cm^2)	S_{calc}	f_{exp} (10^{-6})	f_{calc}
$^3H_6 + {}^5G_5$	362	6.25	5.39	20.28	17.49	6.47	5.41	20.98	17.55
$^5G_5$	418	2.1	2.12	5.9	5.92	3.08	3.08	8.65	8.65
$^5F_1 + {}^5G_6$	451	33.6	33.7	87.5	87.82	32.8	32.9	85.48	85.87
$^5K_8 + {}^5F_2$	469	1.28	1.28	3.29	3.20	129.	1.27	3.12	3.18
$^5F_4 + {}^5S_2$	540	2.93	2.91	6.36	6.32	3.21	3.23	6.99	7.03
$^5F_5$	642	2.73	2.88	5.00	5.26	3.40	3.58	6.23	6.55
$^5I_6$	1170	1.6	1.77	1.61	1.78	1.75	1.75	1.76	1.76
$^5I_7$	1980	4.25	4.21	2.52	2.50	4.24	4.26	2.51	2.52
		rmsΔS = 0.40		rmsΔf = 1.264		rmsΔS = 0.48		rmsΔf = 1.551	

Table 6
The calculated radiative transition rates, the branching ratios and the radiative lifetimes for different transition levels of Ho^{3+}:$NaY(WO_4)_2$ crystal.

Start levels	Terminal levels	Wavelength (nm)	A_σ (s^{-1})	A_π (s^{-1})	A (s^{-1})	β	τ_r(μs)
$^1D_2$	$^3H_6$	359	18540	37680	24920	0.2	8.03
	$^3F_4$	451	86810	74150	82590	0.663	
	$^3H_5$	509	184	479	282	0.002	
	$^3H_4$	653	6625	7154	6801	0.055	
	$^3F_3 + {}^3F_2$	752	9244	8795	9094	0.073	
	$^1G_4$	1502	868	737	824	0.007	
$^1G_4$	$^3H_6$	473	4101	4265	4155	0.521	125.4
	$^3F_4$	643	374	684	477	0.06	
	$^3H_5$	770	1891	2941	2241	0.281	
	$^3H_4$	1156	884	971	913	0.114	
	$^3F_3 + {}^3F_2$	1514	151	273	191	0.024	
$^3H_4$	$^3H_6$	822	4021	4417	4153	0.898	216.3
	$^3F_4$	1432	381	452	404	0.087	
	$^3H_5$	2309	59	85	67	0.015	
$^3F_4$	$^3H_6$	1990	867	633	789	1	1267.4

Transition		λ (nm)	A_σ (s^{-1})	A_π (s^{-1})	A (s^{-1})	β	τ_r (μs)
$^5I_7\rightarrow$	$^5I_8$	2070	195	164	185	1	5405
$^5I_6\rightarrow$	$^5I_7$	2934	48	50	49	0.11	2242
	$^5I_8$	1210	398	394	397	0.89	
$^5I_5\rightarrow$	$^5I_6$	3831	22	24	23	0.06	2617.8
	$^5I_7$	1662	204	198	202	0.529	
	$^5I_8$	899	155	160	157	0.411	
$^5I_4\rightarrow$	$^5I_5$	4472	19	19	19	0.076	4000
	$^5I_6$	2064	100	98	99	0.396	
	$^5I_7$	1211	111	107	110	0.44	
	$^5I_8$	749	22	21	22	0.088	
$^5F_5\rightarrow$	$^5I_4$	4658	0.156	0.202	0.171	/	133
	$^5I_5$	2282	23	23	23	0.003	
	$^5I_6$	1430	278	302	286	0.038	
	$^5I_7$	961	1381	1660	1474	0.196	
	$^5I_8$	645	5302	6603	5735	0.763	
$^5S_2\rightarrow$	$^5F_5$	3330	1.422	1.96	1.601	/	163.6
	$^5I_4$	1942	101	104	102	0.017	
	$^5I_5$	1354	99	98	99	0.016	
	$^5I_6$	1000	423	445	430	0.07	
	$^5I_7$	746	2206	2093	2168	0.355	
	$^5I_8$	540	3370	3198	3313	0.542	

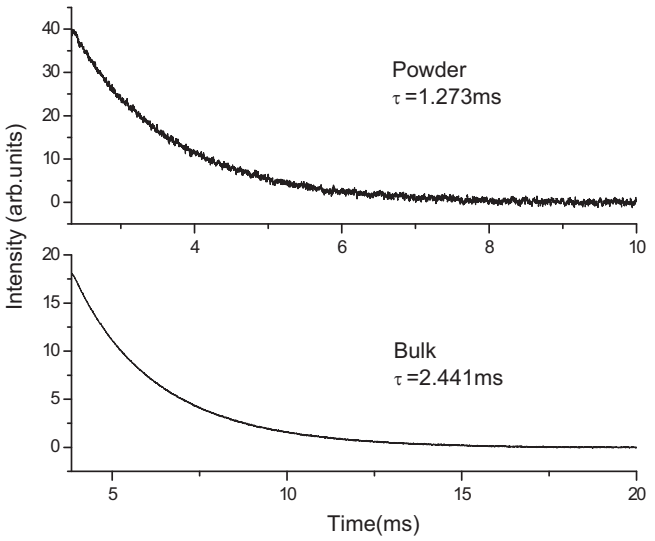

Fig. 5. Decay curves of $^3F_4$ manifold in the samples of bulk and powder in the Tm^{3+} doped $NaY(WO_4)_2$ crystals.

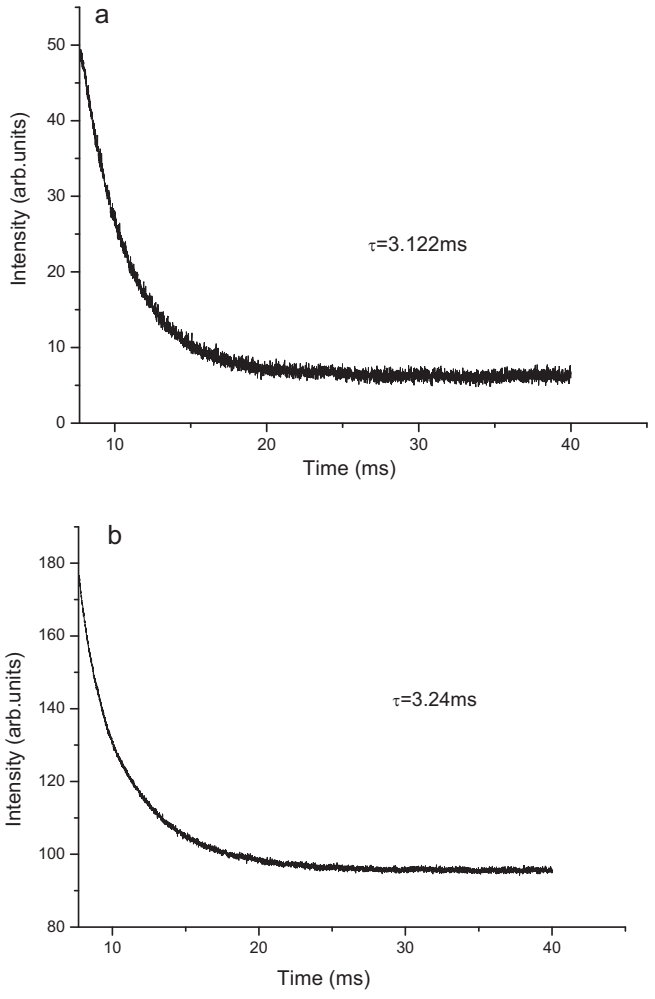

Fig. 6. Decay curves of Ho: $^5I_7$ level in the (a) samples of bulk and powder in the Ho^{3+}:$NaY(WO_4)_2$ and (b) Tm, Ho: $NaY(WO_4)_2$ crystals.

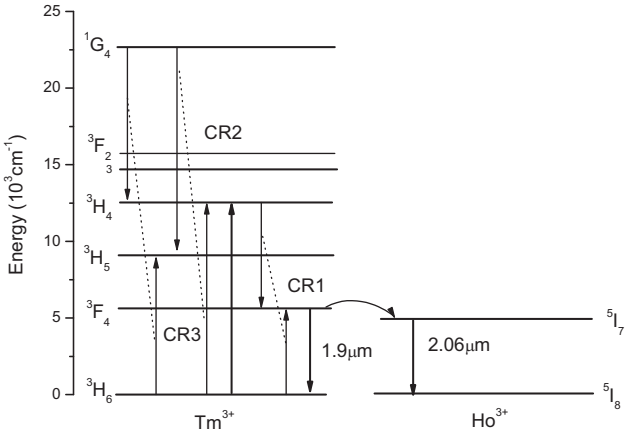

Fig. 7. Energy level diagrams for Tm^{3+} and Ho^{3+}. The continuous arrows show absorption and emission transitions, while dashed arrows show non-radiative transition and energy transfer processes. CR1: $^3H_4 + {}^3H_6 \rightarrow {}^3F_4 + {}^3F_4$, CR2: $^1G_4 + {}^3H_6 \rightarrow {}^3H_5 + {}^3H_4$, CR3: $^1G_4 + {}^3H_6 \rightarrow 3H_4 + {}^3H_5$.

The above data thus support the likelihood of low-threshold and efficient laser operation in Tm^{3+}-, Ho^{3+}-doped $NaY(WO_4)_2$ crystals. We have already obtained a 2.07 μm laser with the Tm, Ho:$NaY(WO_4)_2$ crystal using the fiber-couple 795 nm LD pumped at 283 K. The highest output power was up to 2.7 W. The overall optical conversion efficiency was 5.4% and the slop efficiency was 26% [17].

3.4. Analysis

The energy level scheme and energy transfer processes of Tm^{3+} and Ho^{3+} are shown in Fig. 7 to help interpret the result. After absorbing one pump photon, two ground-level Tm^{3+} ions can be excited to the upper laser level $^3F_4$ multiplet, through a very efficient cross-relaxation process ($^3H_4 + {}^3H_6 \rightarrow {}^3F_4 + {}^3F_4$) if the doping concentration is high enough. This mechanism can be so efficient that at high doping density (say at least 5–8%) the lifetime of $^3H_4$ becomes as short as a few μs and that one excited $^3H_4$ state is converted into two $^3F_4$ states. The 1.9 μm laser emission occurs via the $^3F_4 \rightarrow {}^3H_6$ transition of Tm^{3+}. The $^3F_4$ level of Tm^{3+} is close in energy to the Ho upper laser level $^5I_7$. And it may transfer its excitation to Ho $^5I_7$ multiplet by a resonant or nonresonant energy transfer process from which the 2.06 μm laser originates [34,35].

Fig. 8 shows the scheme of up-conversion processes of Tm^{3+} $^3H_4$ level. The $^3H_4$ multiplet can be efficiently pumped by AlGaAs laser diodes at around 800 nm, then part of Tm^{3+} ions in the $^3H_4$ level can populate to the $^3H_5$ level through a non-radiative relaxation. Absorbing another pump photon, the Tm^{3+} is then excited to the $^1G_4$. $^1G_4$ multiplet could be populated through a possible process: $^3H_4 + {}^3H_5 \rightarrow {}^3H_6 + {}^1G_4$. At the same time part of the Tm^{3+} on the $^1G_4$ multiplet relaxes to the $^3F_{2,3}$ multiplets. Tm^{3+} also can populated $^1D_2$ multiplet from $^3F_{2,3}$ by absorbing a pump photon. Clearly, the up-conversion processes will bring out loss and reduce the pumping efficiency. The main disadvantage of Tm^{3+} as a quasi-three-level system for the $^3F_4 \rightarrow {}^3H_6$ laser transition is the thermal population of the terminal level, and strong pump power to meet the higher threshold requirements. Higher ion concentration could improve pump efficiency, but with the increase of ion concentration, conversion loss also increases [1,23]. Thence, the laser performance critically depends on the activation of ion concentration, operation temperature and gain medium size, etc. Therefore, we need to find the optimal conditions, which is our continuous research work.

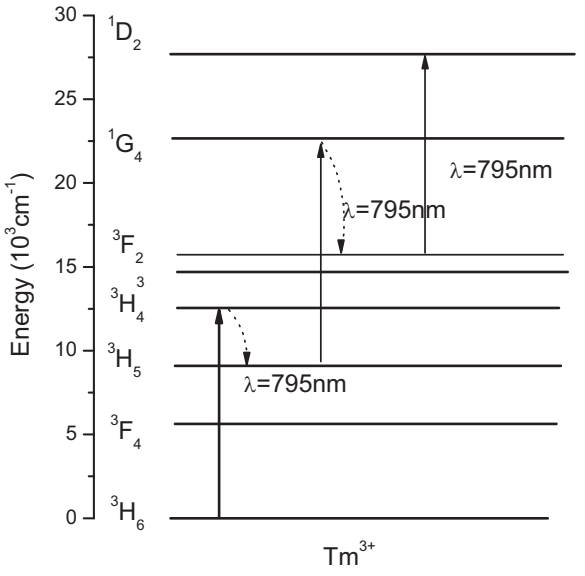

Fig. 8. The diagram of Tm^{3+} up-conversion process of $^3H_4$ exciting level.

4. Conclusion

Tm^{3+}, Ho^{3+} singly doped and Tm^{3+}/Ho^{3+} co-doped $NaY(WO_4)_2$ crystals were grown successfully by Czochralski method. The absorption spectra were measured at room temperature. The broad absorption band and relative high absorption cross section around 796 nm are suitable for laser diode pumping. We calculated the stimulated emission cross sections around 2.0 μm by the reciprocity method. The maximum emission cross sections are 2.16×10^{-20} cm^2 at 1.795 μm and 1.43×10^{-21} cm^2 at 2.047 μm in Tm- and Ho-doped $NaY(WO_4)_2$ crystals in σ polarization, respectively. The room temperature emission spectra were recorded. The $^3F_4 \rightarrow {}^3H_6$ (Tm^{3+}) and $^5I_7 \rightarrow {}^5I_8$ (Ho^{3+}) IR transitions are broad emission bands at about 2.0 μm. Using fine powder of the crystals for recording the decay time can efficiently decline the radiative-trapping. The results show that these crystals may be preferable candidates for tunable IR laser material at 1.9–2.1 μm. The Tm^{3+} laser performance depends on the concentration of the activating ion, operation temperature and gain medium size, etc. Therefore, finding the optimal conditions is our continuous research work to be carried out.

Acknowledgments

This research was supported by National Nature Science Foundation of China (No. 50902129, 61078076), major projects from FJIRSM (SZD09001), major directional projects from Chinese Academy of Sciences (KJCX2-EW-H03), Fund of Key Laboratory of Optoelectronic Materials Chemistry and Physics and Chinese Academy of Sciences (2008DP173016), Science and Technology Plan Major Project of Fujian Province of China (Grant no. 2010I0015) and Fund of Research Center of Laser Technology Integration and Application Engineering Technology of Haixi Industrial Technology Research Institute (2009H2009).

References

[1] B.M. Walsh, Laser Phys. 19 (2009) 855–866.
[2] K. Scholle, E. Heumann, G. Huber, Laser Phys. Lett. 1 (2004) 285–290.
[3] I. Bottrill, D.F. Perrault, M.P. Michail, S.P. Dennis, Proc. SPIE 2128 (1994) 23–30.
[4] H.P. Weber, M. Frenz, H. Pratisto, M. Ith, R. Hausler, P. Schar, Laser Phys. 8 (1998) 785–793.
[5] T. Schweizer, B.N. Samson, J.R. Hector, W.S. Brocklesby, D.W. Hewak, D.N. Payne, Infrared Phys. Technol. 40 (1999) 329–335.
[6] R. Kaufman, A. Hartmann, R. Hibst, Dermatol. J. Surg. Oncol. 20 (1994) 112–118.
[7] J.M. Cano-Torres, X. Han, A. Garcia-Cortes, M.D. Serrano, C. Zaldo, F.J. Valle, X. Mateos, S. Rivier, U. Griebner, V. Petrov, Mater. Sci. Eng. B 146 (2008) 22–28.
[8] E.P. Chicklis, C.S. Naiman, R.C. Folweiler, D.R. Gabbe, H.P. Jenssen, A. Linz, Appl. Phys. Lett. 19 (1971) 119–121.
[9] L.F. Johnson, G.D. Boyd, K. Nassau, Proc. IRE 50 (1962) 86–87.
[10] J.A. Caird, L.G. DeShazer, J. Nella, J. Quant. Electron. 11 (1975) 874.
[11] K.S. Lai, P.B. Phua, R.F. Wu, Y.L. Lim, E. Lau, S.W. Toh, B.T. Toh, A. Chng, Opt. Lett. 25 (2000) 1591–1593.
[12] X.M. Han, J.M. Cano-Torres, M. Rico, C. Cascales, C. Zaldo, X. Mateos, S. Rivier, U. Griebner, V. Petrov, J. Appl. Phys. 103 (2008) 083110.
[13] K. Ohta, H. Saito, M. Obara, J. Appl. Phys. 73 (1993) 3149.
[14] N. Coluccelli, D. Gatti, G. Galzerano, F. Cornacchia, D. Parisi, A. Toncelli, M. Tonelli, P. Laporta, Appl. Phys. B 85 (2006) 553.
[15] Z.L. Zhu, Y.N. Qian, J.H. Liu, Y.C. Wan, L. Zhang, J. Ceram. Soc. 35 (2007) 991–994.
[16] C. Cascales, M.D. Serrano, F. Esteban-Betegón, C. Zaldo, R. Peters, K. Petermann, G. Huber, L. Ackermann, D. Rytz, C. Dupre, M. Rico, J. Liu, U. Griebner, V. Petrov, Phys. Rev. B 74 (2006) 174114.
[17] F.G. Yang, C.L. Sun, Z.Y. You, C.Y. Tu, G. Zhang, H.Y. Zhu, Laser Phys. 20 (2010) 1695–1697.
[18] B.R. Judd, Phys. Rev. 127 (1962) 750–761.
[19] G.S. Ofelt, J. Chem. Phys. 37 (1962) 511–520.
[20] W.T. Carnall, P.R. Fields, K. Rajnak, J. Chem. Phys. 49 (1968) 4424.
[21] V. Petrov, F. Güell, J. Massons, J. Gavalda, R.M. Sole, M. Aguiló, F. Diaz, U. Griebner, IEEE J. Quant. Electron. 40 (2004) 1244.
[22] H.P. Jenssen, A. Linz, R.P. Leavitt, C.A. Morrison, D.E. Wortman, Phys. Rev. B 11 (1975) 92.
[23] W.J. Guo, Y.J. Chen, Y.F. Lin, Z.D. Luo, X.H. Gong, Y.D. Huang, J. Appl. Phys. 103 (2008) 093106.
[24] L. Macalik, J. Hanuza, D. Jaque, J.G. Solé, Opt. Mater. 28 (2006) 980.
[25] F. Güell, J. Gavaldà, R. Solé, M. Aguiló, F. Diaz, M. Galan, J. Massons, J. Appl. Phys. 95 (2004) 919.
[26] S.N. Bagaev, S.M. Vatnik, A.P. Maiorov, A.A. Pavlyuk, D.V. Plakushchev, IEEE J. Quant. Electron. 30 (2004) 310.
[27] O. Silvestre, M.C. Pujol, F. Güell, M. Aguiló, F. Díaz, A. Brenier, G. Boulon, Appl. Phys. B 87 (2007) 111–117.
[28] Y. Wei, C. Tu, H. Wang, F. Yang, G. Jia, Z. You, X. Lu, J. Li, Z. Zhu, Y. Wang, J. Alloy Compd. 438 (2007) 310–316.
[29] H. Wang, J. Li, G. Jia, Z. You, F. Yang, Y. Wei, Y. Wang, Z. Zhu, X. Lu, C. Tu, J. Alloy Compd. 431 (2007) 277–281.
[30] X. Lu, Z. You, J. Li, Z. Zhu, G. Jia, B. Wu, C. Tu, J. Alloy Compd. 458 (2008) 462–466.
[31] X. Ma, Z. You, Z. Zhu, J. Li, B. Wu, Y. Wang, C. Tu, J. Alloy Compd. 465 (2008) 406–411.
[32] Y. Yang, B. Yao, B. Chen, C. Wang, G. Ren, X. Wang, Opt. Mater. 29 (2007) 1159–1165.
[33] J.S. Liao, Y.F. Lin, Y.J. Chen, Z.D. Luo, E. Ma, X.H. Gong, Q.G. Tan, Y.D. Huang, J. Opt. Soc. Am. B 23 (2006) 2572–2580.
[34] F. Cornacchia, A. Toncelli, M. Tonelli, Quant. Electron. 33 (2009) 61–109.
[35] A.A. Lagatsky, F. Fusari, S.V. Kurilchik, V.E. Kisel, A.S. Yasukevich, N.V. Kuleshov, A.A. Pavlyuk, C.T.A. Brown, W. Sibbett, Appl. Phys. B 97 (2009) 321–326.